iScience

CellPress

Article

Application of Stable Isotope Tracing to Elucidate Metabolic Dynamics During *Yarrowia lipolytica* α-Ionone Fermentation

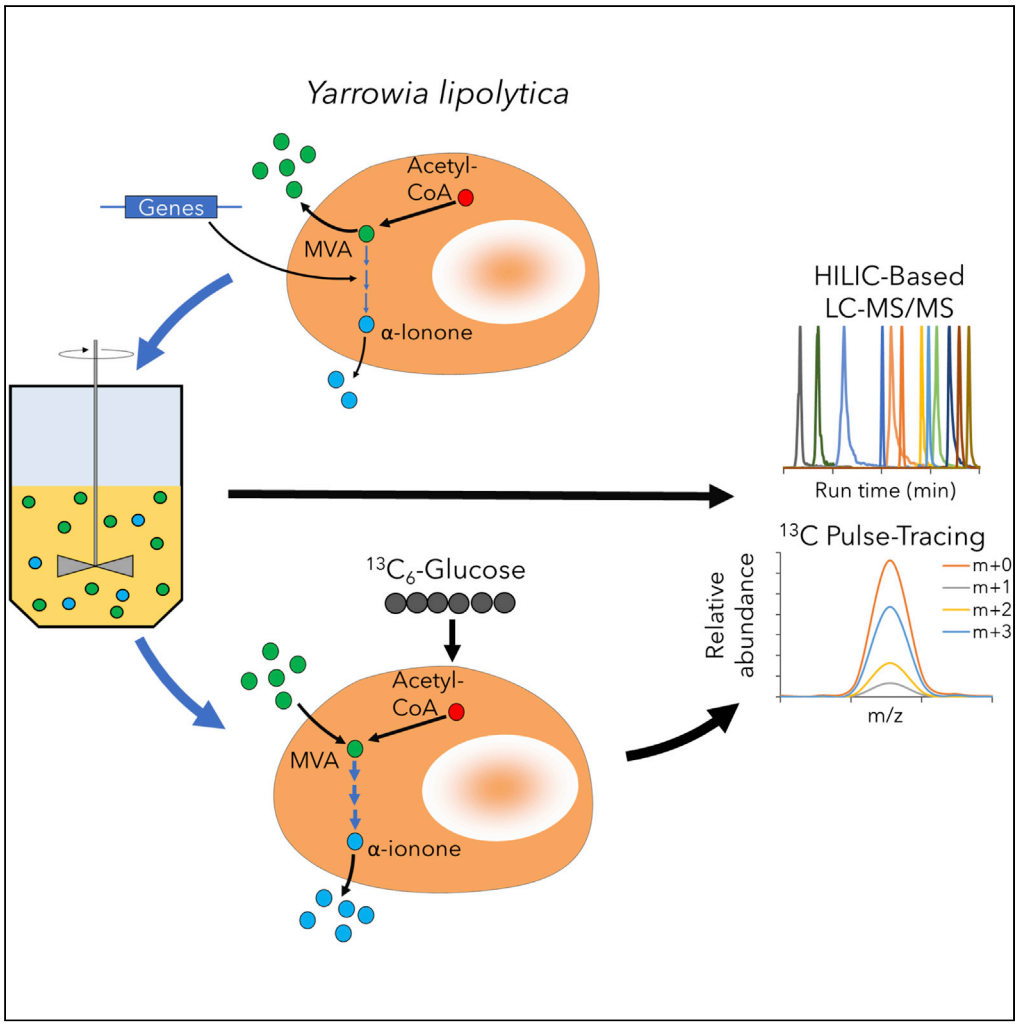

Jeffrey J. Czajka, Shrikaar Kambhampati, Yinjie J. Tang, Yechun Wang, Doug K. Allen

yinjie.tang@seas.wustl.edu (Y.J.T.)
ywang@arch-innotek.com (Y.W.)
doug.allen@usda.gov (D.K.A.)

HIGHLIGHTS

A HILIC method is demonstrated for efficient separation of 57 cellular metabolites

Production of α-ionone was ~400 mg/L in bench-top bioreactors

Engineered *Y. lipolytica* secreted then consumed mevalonate during fermentation

Oxidative phosphorylation may limit performance in high-cell-density fermentations

Czajka et al., iScience *23*, 100854
February 21, 2020
https://doi.org/10.1016/j.isci.2020.100854

iScience

CellPress

Article

Application of Stable Isotope Tracing to Elucidate Metabolic Dynamics During *Yarrowia lipolytica* α-Ionone Fermentation

Jeffrey J. Czajka,[1,5] Shrikaar Kambhampati,[2,5] Yinjie J. Tang,[1,*] Yechun Wang,[4,*] and Doug K. Allen[2,3,6,*]

SUMMARY

Targeted metabolite analysis in combination with ^{13}C-tracing is a convenient strategy to determine pathway activity in biological systems; however, metabolite analysis is limited by challenges in separating and detecting pathway intermediates with current chromatographic methods. Here, a hydrophilic interaction chromatography tandem mass spectrometry approach was developed for improved metabolite separation, isotopologue analysis, and quantification. The physiological responses of a *Yarrowia lipolytica* strain engineered to produce ~400 mg/L α-ionone and temporal changes in metabolism were quantified (e.g., mevalonate secretion, then uptake) indicating bottleneck shifts in the engineered pathway over the course of fermentation. Dynamic labeling results indicated limited tricarboxylic acid cycle label incorporation and, combined with a measurable ATP shortage during the high ionone production phase, suggested that electron transport and oxidative phosphorylation may limit energy supply and strain performance. The results provide insights into terpenoid pathway metabolic dynamics of non-model yeasts and offer guidelines for sensor development and modular engineering.

INTRODUCTION

Liquid chromatography-tandem mass spectrometry (LC-MS/MS)-based metabolite quantification is increasingly useful to guide metabolic engineering, and when paired with ^{13}C-isotopic tracing methods it can be used to track fluxes through metabolism and carbon movement (Jang et al., 2018; Abernathy et al., 2019; Allen, 2016). The molecular measurements give insight into the status of engineered cellular systems, facilitating further strain improvement and greatly reducing the time spent developing industrial production strains (Campbell et al., 2017). Metabolic measurements from bioreactors at production scale can identify nonuniformities such as imperfect mixing, fluctuations in pH, and temperature and substrate gradients, phenomena that can lead to suboptimal strain performance and enhanced rates of genetic mutation (Käß et al., 2014; Elena and de Visser, 2003). Thus, detection of metabolic changes that are a result of large-scale cultivations (such as alterations in metabolite bottlenecks or low oxidative phosphorylation efficiency) enables more robust industrial strain designs or fermentation optimizations (Wehrs et al., 2019). However, production-scale reactors are not readily available and are cost-prohibitive. Therefore, scaled-down bench-top fermenters provide a compromise to rigorously assess initial strain performance.

Analytically, MS-based ^{13}C-isotopic tracing methods and, more generally, metabolite profiling analyses cannot accurately identify and quantify all metabolites within a single run due to challenges in separation and detection. Best practices use gas chromatography (GC) or LC in tandem with MS to separate and quantify a subset of metabolites including isotopologues. GC is useful for metabolite quantification but requires a derivatization step (via silylation or alkylation) to volatilize polar sugars, amino acids, and organic acids and results in reduced sample stability (Halket et al., 2005; Allen and Ratcliffe, 2009). LC does not require chemical modification of analytes, but the presence of sample matrix and solvent effects can suppress ion signals. In some instances, the signals can be enhanced with the addition of an ion pairing (IP) reagent; however, the IP reagent is present at millimolar quantities in the buffer and contaminates instrumentation, requiring considerable effort in post-operation cleanup. Hydrophilic interaction chromatography (HILIC) columns and methods separate amino acids (Kambhampati et al., 2019), sugars (Xia et al., 2019), and central carbon intermediates (Rodriguez et al., 2016; Teleki et al., 2015) and are now used for targeted metabolite quantification in conjunction with dynamic ^{13}C-tracing to examine *Escherichia coli* and cyanobacteria metabolic dynamics (Li et al., 2017; Gao et al., 2016b). In the current study, a HILIC method using the modifier medronic acid was developed and employed to retain and separate isobaric metabolites within a single 20-min run. Limits of detection were determined for 15 amino acids and 42 metabolite intermediates of

[1]Department of Energy, Environmental and Chemical Engineering, Washington University, St. Louis, MO, USA

[2]Donald Danforth Plant Science Center, St. Louis, MO, USA

[3]United States Department of Agriculture, Agricultural Research Service, St. Louis, MO, USA

[4]Arch Innotek, LLC, 4320 Forest Park Avenue, St Louis, MO, USA

[5]These authors contributed equally

[6]Lead Contact

*Correspondence: yinjie.tang@seas.wustl.edu (Y.J.T.), ywang@arch-innotek.com (Y.W.), doug.allen@usda.gov (D.K.A.)

https://doi.org/10.1016/j.isci.2020.100854

This is an open access article under the CC BY-NC-ND license (http://creativecommons.org/licenses/by-nc-nd/4.0/).

the central carbon metabolism and mevalonate (MVA) pathway. The developed HILIC method and MS/MS were used to analyze an oleaginous yeast *Yarrowia lipolytica* strain engineered to produce α-ionone.

Ionones are a subclass of terpenoid aroma compounds in plants that are valuable to the fragrance and flavor industries. Typically, plants only produce low amounts of aroma compounds. These low natural levels combined with increasing consumer demand for all-natural products has strained the current ionone supply chain and provided an opportunity for the development of new production methodologies. Recent efforts have focused on producing ionones via biotechnological processes (Jiang et al., 2019; Zhang et al., 2018; Chen et al., 2019), including a study reporting titers of approximately 400 mg/L of α-ionone from *E. coli* in 10,000-L fermenters (Lukin et al., 2019). However, organisms that are Generally Recognized As Safe (GRAS) are desirable. *Y. lipolytica* is an oleaginous yeast that is capable of accumulating large amounts of lipids and fatty acids (>70% dry cell weight (DCW), after genetic engineering, Friedlander et al., 2016; Xu et al., 2016). The large flux through acetyl-CoA and the ability to consume a wide range of substrates suggest that *Y. lipolytica* may be well suited for terpene production. Previously, a strain was engineered for the production of β-ionone (Czajka et al., 2018). Here, a *Y. lipolytica* strain engineered to produce α-ionone is described in high-cell-density fermentations. Using HILIC-MS/MS, temporal shifts in metabolism, which resulted in MVA excretion during the growth phase followed by uptake during the ionone production phase, were captured over the course of fermentation. Labeling measurements from pulse-trace experiments indicated that tricarboxylic acid (TCA) cycle activity was limited under high-cell-density fermentations, re-capitulating a trend previously described in *E. coli* (Chen et al., 2011). The findings here have broad implications for the metabolic engineering community, as the MVA pathway is the source of a number of valuable natural compounds.

RESULTS

Metabolite Detection via HILIC Method

A comprehensive HILIC method was developed to detect and achieve efficient separation of sugar phosphates, sugars, and organic acids in central carbon metabolism; intermediates in the MVA pathway; and amino acids within a single, 20-min run. The aqueous running buffer contained 10 mM ammonium acetate (pH 9.0) in water (buffer A), and the organic buffer contained 10 mM ammonium acetate (pH 9.0) in acetonitrile:water (9:1) (buffer B); 5 μM medronic acid ($CH_6O_6P_2$) was added to both buffers. The binary gradient started at 95% B and was gradually reduced over a 20-min run time that included 6 min of equilibration back to the starting conditions (described in the Methods). Limits of detection of 17 sugar phosphates, 7 sugars, 8 organic acids, 7 MVA pathway intermediates, 15 amino acids, and the energy molecules (adenosine triphosphate [ATP], adenosine diphosphate [ADP], and adenosine monophosphate [AMP]) were quantified. The chromatographic separation for a select set of metabolites relevant to this study is presented in Figure 1. A complete list with retention times, limits of detection, and MS parameters is provided in Table S1.

One challenge with the detection and quantification of central carbon intermediates is that a number of important metabolites are isomers. Triose phosphates (glyceraldehyde-3-phosphate and dihydroxyacetone phosphate), pentose phosphates (ribose-5-phosphate and ribulose-5-phosphate), hexose phosphates (glucose-1-phosphate, fructose-6-phosphate, and glucose-6-phosphate), and some sugars/alcohols (glucose and fructose, sucrose, maltose, galactinol, etc.) are not distinguishable from each other by MS because of identical chemical formulas. Chromatographic separation of these isobaric compounds was achieved using HILIC and alkaline pH conditions (pH 9.0) (Figure 1A), with the exception of the pentose phosphates (quantified as pentose-5-phosphates). Medronic acid and a slow initial solvent gradient (95%–70% buffer B over 8 min) played a crucial role in the sensitive detection and resolution of sugar phosphates and MVA pathway intermediates (Figures 1B and 1C). The optimal peak shapes resulted in lower limits of detection (<5 pmol) sufficient for quantification. The HILIC method was then verified with a yeast production system, *Y. lipolytica*, engineered to produce α-ionone. As the yeast was cultivated in rich medium (YPD) that contains peptone, the amino acids were not monitored. ^{13}C-isotopic tracing methods were employed with the resulting isotope measurements collected via a scheduled multiple reaction monitoring (MRM) method.

Yarrowia lipolytica Engineering for α-Ionone Production

Arch Innotek's proprietary *Y. lipolytica*-producing α-ionone strain was used throughout the study. The strain was established based on a β-ionone-producing *Y. lipolytica* strain previously described (Czajka

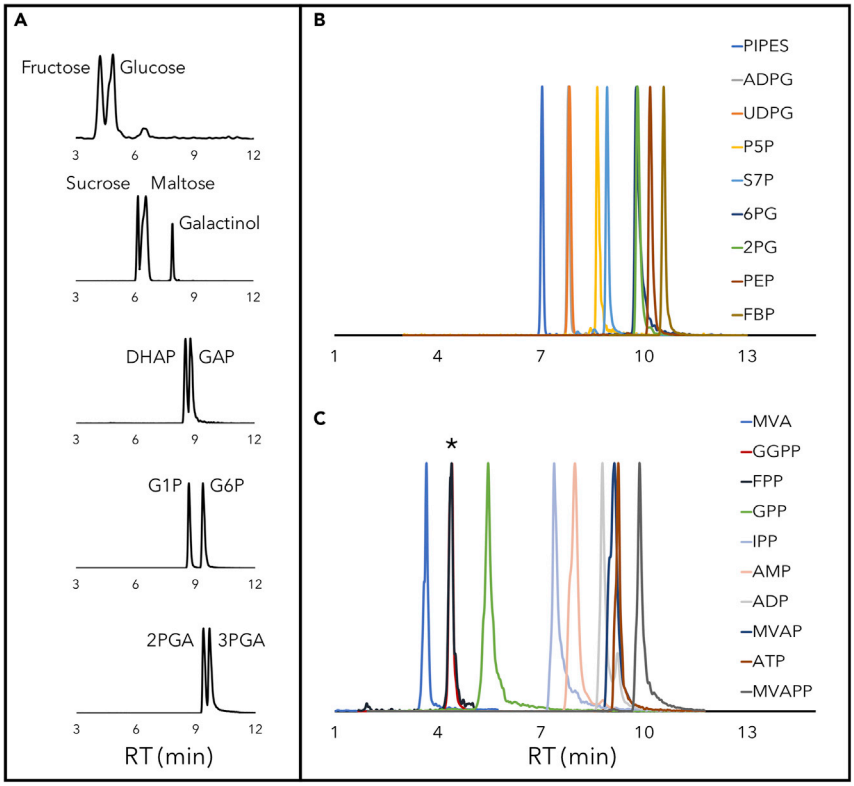

Figure 1. HILIC Metabolite Peaks

(A–C) (A) Isobaric sugars and sugar phosphates, (B) central carbon metabolite intermediates, and (C) MVA pathway intermediates. *FPP and GGPP eluted at approximately the same time.

et al., 2018). The α- and β-ionone production pathways share 12 common biosynthetic steps through the MVA pathway (Zhang et al., 2018). Three molecules of acetyl-CoA are condensed to form 3-hydroxy-3-methylglutaryl-CoA, which is then converted to the five-carbon terpene building blocks isopentyl-pyrophosphate (IPP) and dimethylallyl pyrophosphate (DMAPP). IPP and DMAPP are sequentially condensed to form the C_{40} compound, lycopene, the last shared intermediate between the ionone isomer pathways. For α-ionone, the ends of the same lycopene molecule are chemically linked to form δ- (one ring) or ε- (two rings) carotene. The introduction of lycopene cyclase from *Lactuca sativa* (LsLCYe) and the carotene cleavage dioxygenase from *Osmanthus fragrans* (OfCCD1) (Wang, 2019) led to the detectable production of α-ionone. When the two genes were added to a previously constructed and described strain engineered to overexpress the MVA pathway (Table S2; Czajka et al., 2018), a titer of 43 ± 3 mg/L of α-ionone was achieved in shake-flask growths (Figures S1 and S2). Strains used in this study and their genetic information are presented in Table S2.

Bench-Top Fermentation Achieved ~400 mg/L of α-Ionone

A bench-top bioreactor (Sartorius BIOSTAT A, 5 L) was operated in fed-batch mode with a 10% (v/v) dodecane layer to extract, retain, and quantify ionone titers. A representative fermentation curve is shown in Figure 2A. The maximal biomass, measured by OD_{600}, was achieved within 75 h. The dissolved oxygen saturation percentage dropped to ~2%–5% during the early growth phase and maintained this low level until the late production phase (~150 h). The residual glucose concentration is shown in Figure S3. α-Ionone was produced throughout the entire fermentation period; however, there was an increase in the average production rate from 0.9 ± 0.5 mg/L/h to 3.7 ± 0.4 mg/L/h (Figure 2B) at 104 ± 10 h after inoculation. 408 ± 50 mg/L of α-ionone was obtained at the end of the fermentation, among the highest reported titers to date (Figure 2C). The ratio of α- to β-ionone was 90% ± 2%, with 80% ± 5% of the quantified ionone in the dodecane overlay (i.e., ~20% remained intracellular). Previously, it was shown that the ionone capture efficiency of a dodecane overlay is <100% (~76%), thus the reported α-ionone production estimate is

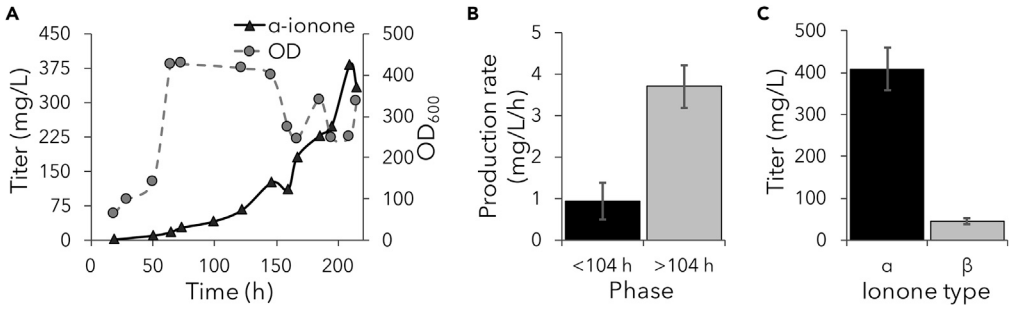

Figure 2. Ionone Production Parameters in 5-L Bioreactor

(A–C) (A) Representative OD_{600} and α-ionone production over time, (B) α-ionone production rate before and after 104 h, and (C) final titers of α- and β-ionones at the end of 5-L bioreactor cultivation. Data are represented as mean ± SD from biological triplicates.

conservative (Czajka et al., 2018). Based on the strain fermentation characteristics, metabolic changes due to pathway engineering and product synthesis were further investigated.

Metabolite Comparisons and Isotopic Pulse-Chase Indicated Minimal Changes to the Flux Profile

Engineering the overexpression of multi-step enzymatic pathways can lead to metabolic burdens and unforeseen metabolic changes. To determine the cellular response to the engineered pathway, intracellular metabolite concentrations (pool sizes) were measured in exponentially growing cells (in shake-flasks) via targeted metabolite analysis. A comparison with the wild-type (WT) indicated that the engineered strain had reduced TCA cycle pool sizes (Figures 3A and 3B). Previous studies have also reported reduced levels of citrate (CIT) and other TCA intermediates during shake-flask cultivations of strains producing carotenoids (Zhao et al., 2017; Nagai et al., 2018), as a consequence of re-routing of TCA cycle carbon to product synthesis (through the ATP-citrate lyase reaction or acetyl-CoA competition). To minimize the competition for TCA intermediates, glutamate, acetate, and ethanol were supplemented to shake-flask cultures. Interestingly, only ethanol resulted in an increase of α-ionone titer (Figure S2), consistent with previous results for a beta carotene-producing strain (Czajka et al., 2018). Isotopic tracing was then used to compare the pathway activity of the WT and engineered strains during fermentation processes.

Cells from fed-batch bioreactors were collected over the course of fermentation and immediately pulsed into a medium containing fully labeled (U-$^{13}C_6$) glucose in shake-flasks. After a specified time in the labeled medium, cells were mixed with a cold ethanol:sodium chloride solution (final solution temperature ~ −20°C) to rapidly quench cell metabolism (Figure S4). The dynamic labeling results revealed four main observations. First, the central carbon-labeling profiles were reproducible across bioreactor runs (Figures 3 and S5). Second, the incorporation of ^{13}C into TCA cycle metabolites (CIT, α-ketoglutarate [AKG], succinate [SUC], malate [MAL]) in both WT and engineered strains was much lower relative to the sugar phosphates in both growth and production phases (Figures 3, S5, and S6). Third, the MVA labeling enrichment was higher in cells from the growth phase than in those from the production phase (Figure S5). Fourth, MVA was labeled to lower levels in the engineered strain relative to the WT (Figure 3). Extending the labeling period from 20 min to 2 h did not result in significant MVA labeling (Figure S5). As the engineered strain had an overexpressed MVA pathway, MVA labeling enrichment was expected to be higher than in the WT, yet the opposite was found to be the case. Therefore, additional metabolite quantification was performed.

Extracellular MVA Quantification Indicates MVA Uptake from the Media and a Shifting Metabolic Bottleneck

Metabolite concentrations in the fermentation medium of the engineered strain were quantified to gain insights into the low MVA ^{13}C incorporation and to understand the metabolic shifts over the course of the fermentation. A significant amount of MVA secretion was identified, with concentrations peaking at 405 ± 33 mg/L (Figure 4). In a separate test, MVA was also secreted during fermentation without a dodecane overlay and reached ~270 mg/L, indicating that the secretion is inherent to the biological system and not an artifact of the dodecane overlay. The MVA concentration decreased following the peak, with a

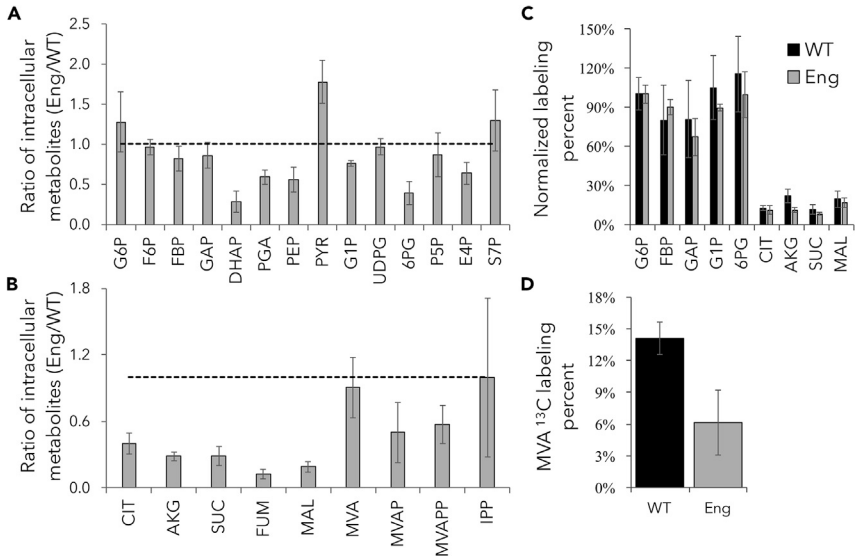

Figure 3. WT and Engineered Strain Pool Size Comparisons and Pulse-Trace Results

(A) Intracellular metabolite pool size ratios of the upper glycolysis pathway metabolites of the engineered strain compared with the WT.

(B) Pool size ratios of the TCA cycle and MVA pathway metabolites. The dotted line shows a ratio of 1 and represents the metabolites that have equal pool sizes in each strain.

(C) Pulse-trace labeling incorporation. ^{13}C content of central carbon metabolites after 20 min of metabolite labeling using a U-$^{13}C_6$ glucose tracer for wild-type (WT) and engineered (Eng) strains. Labeling percentage is normalized to the average G6P labeling.

(D) MVA labeling.

See also Figures S5 and S6. (A and B) Data are represented as mean ± SD from biological triplicates; (C and D) data are represented as mean ± SD from biological duplicates.

corresponding increase in the production of ionone. A similar dynamic was observed for CIT, MAL, SUC, fumarate (FUM), and pyruvate (PYR), which peaked at a total concentration of 4.2 ± 0.9 g/L (Figure 4B). The extracellular metabolite dynamics suggested that secreted MVA, which was unlabeled, was taken up by the yeast cells and used to produce ionone, consistent with the low level of MVA ^{13}C incorporation observed in the engineered strain (Figures 3 and S5). Organic acids have been previously reported to be consumed by *Y. lipolytica* (Papanikolaou et al., 2002; Sabra et al., 2017), whereas MVA consumption has been widely reported in *E. coli* (Yoon et al., 2006; Wang et al., 2011), and to a lesser extent in some yeast (*Rhodotorula glutinis*, Ikeura et al., 1988; *Phaffia rhodozyma*, Calo et al., 1995), but not others (*S. cerevisiae*, Rodriguez et al., 2016). To test whether the engineered *Y. lipolytica* strain was capable of MVA uptake for production of ionone, cultures were grown in shake-flasks and supplemented with 2 g/L MVA. The resulting ionone production, measured via GC-MS, was increased by 35% ($p < 0.05$, Figure S2). The results indicate that MVA can serve as a valuable carbon source for enhanced production of ionone.

Pool Size Quantification Indicated Limited TCA Cycle Efficiency and Energy Limitation

Intracellular pool sizes were measured in the engineered strain during the fermentations. Intracellular MVA concentrations decreased over the course of the fermentation (Figure 5). Of the downstream MVA pathway intermediates, IPP had the highest concentration, geranyl pyrophosphate (GPP) and farnesyl pyrophosphate (FPP) were present in low abundance and geranyl-geranyl pyrophosphate (GGPP) was not present at detectable levels. Of the quantifiable metabolites, MAL, FUM, and AKG were the most abundant (Figure 5).

Most metabolite concentrations declined over the fermentation, with significant decreases occurring during the late production phase (146 h). The intermediates of the TCA cycle had a 2.9-fold (MAL), 3.1-fold (FUM), 3.0-fold (SUC), and 3.5-fold (CIT) reduction between the 98.5- and 146-h samples (Figure 5). The general decrease of metabolites may be the result of reduced metabolic and TCA cycle activity when cells entered the stationary phase. As an obligate aerobe, *Y. lipolytica* relies on the TCA cycle and oxidative

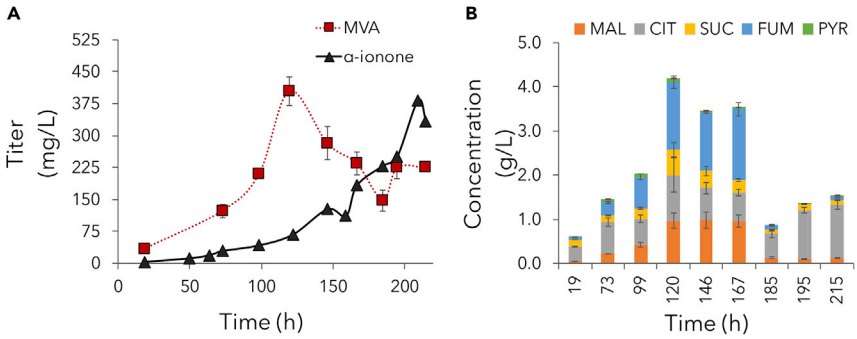

Figure 4. Representative Extracellular Metabolite Dynamics Over the Course of Fermentation

(A and B) (A) MVA and ionone production and (B) organic acids. Error bars represent standard deviation of duplicates. Data are represented as mean ± SD from technical duplicates.

phosphorylation to supply energy required for metabolic activity. Thus, reduced TCA cycle activity and capacity for electron chain transport due to low oxygen availability would be expected to result in energy deficiencies. Indeed, when the concentrations of ATP, ADP, and AMP were measured, the calculated energy charge (defined as ([ATP] + $^1/_2$[ADP])/([ATP]+[ADP]+[AMP]) was significantly lower in the production phase (0.5) relative to the growth phase (0.9) and characteristic of an energy-limited cellular state (Wu et al., 2016); however such numbers should be viewed qualitatively because energy metabolites can be difficult to quantify accurately. A similar reduction in TCA cycle metabolites was observed over time in *Y. lipolytica* lycopene-producing strains (Zhao et al., 2017).

DISCUSSION

Metabolite profiling and isotopic labeling has rapidly become an important tool for analyzing biological systems; however, it is often the limiting analytical step due to challenges in separating compound classes (hydrophobic lipids, polar sugar phosphates, etc.) and detecting pathway intermediates with one short chromatographic method. Reverse-phase chromatography methods have been able to successfully separate many central carbon metabolites using an IP agent, but the extensive cleaning needed to remove the IP modifier is time-consuming. HILIC methods have recently become more widely utilized because of their ability to separate multiple types of compound classes within central carbon metabolism (Li et al., 2016, 2017; Luo et al., 2019; Kambhampati et al., 2019). Alkaline conditions in HILIC methods provide better detection capabilities than acidic conditions (Teleki et al., 2015). A recent study demonstrated that the addition of medronic acid to alkaline conditions in HILIC significantly improved sugar phosphate peak quality (Hsiao et al., 2018). Here, a medronic acid- and alkaline-based HILIC method was developed with a high initial buffer B percent (95%) and slow gradient changes that results in adequate and robust separation of sugar phosphates, sugars, and organic acids in the central and secondary metabolism as well as amino acids. The HILIC method's ability to separate important isobars along with robust methods for quenching cellular metabolism and metabolite extraction were examined in a *Y. lipolytica* strain that produced high titers of α-ionone, in part due to a change in MVA use during ionone production.

Shifts in Metabolism during High-Cell-Density Fermentation Processes Can Result in Unbalanced Production Pathways

Y. lipolytica can naturally produce large quantities of lipids and therefore has the capacity to generate significant amounts of acetyl-CoA, the precursor for the MVA pathway. Thus, *Y lipolytica* can be metabolically engineered for terpene production (Kildegaard et al., 2017; Schwartz et al., 2017; Larroude et al., 2018). However, if the goal is to reach industrial production, the metabolic response to both engineering and high-cell-density fermentations must be considered carefully. Pathway engineering and introduction of heterologous genes can lead to metabolic reorganization in response to cellular burdens that affect strain productivity differently in small-scale (i.e., shake-flasks) growth conditions relative to high-cell-density bioreactors (Sabra et al., 2017). Here, the MVA secretion by the engineered strain during the growth phase and uptake during the production phase suggested that a major metabolic shift occurred and that the production pathway bottleneck changed over the course of fermentation. Although it is possible that the secretion was promoted by the dodecane overlay (an effective extraction solvent for terpenes), an additional

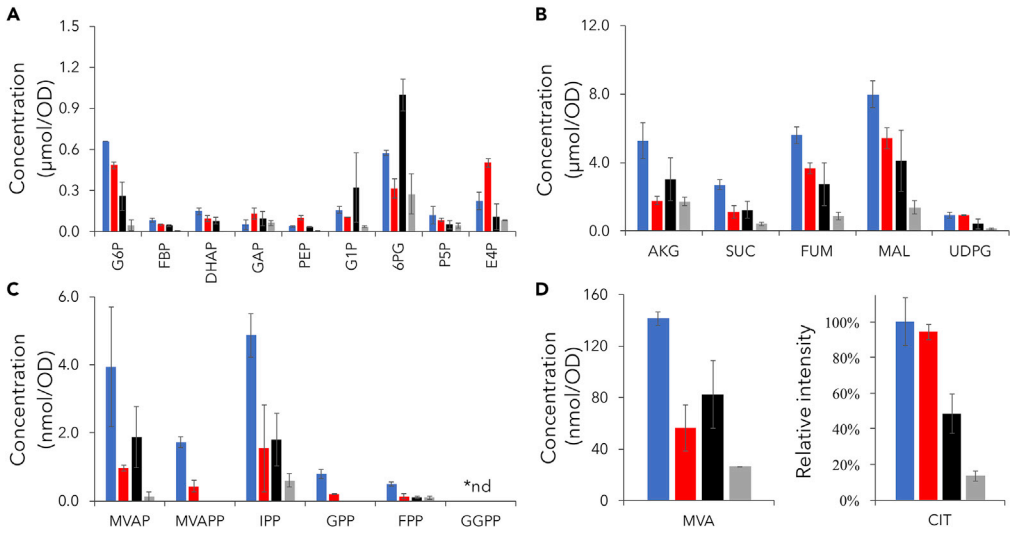

Figure 5. Representative Intracellular Metabolite Concentrations during the 5-L Bioreactor Fermentation

(A–D) (A) Glycolysis and pyrophosphate pathway metabolites, (B) TCA cycle metabolites, (C) MVA pathway metabolites, and (D) MVA concentration and CIT pools reported as relative intensities *nd, not detected. Colors correspond to sampled time points with 50 h (blue), 71 h (red), 98.5 h (black), and 146 h (gray). Data are represented as mean ± SD from technical duplicates.

fermentation without the overlay found that MVA secretion still occurred (albeit at slightly lower levels), ensuring the phenomena was inherent to the biological system. Thus, the secretion of MVA during growth suggests that a downstream enzyme step is initially rate limiting. Some studies have shown that the expression levels of the carotenoid-producing gene remain relatively constant over the course of one cultivation in natural (astaxanthin-overproducing mutant, *Phaffia rhodozyma*) and heterologous (*E. coli*) systems (Miao et al., 2011; George et al., 2018), whereas other reports have indicated that oxygen content and mannitol accumulation can affect gene expression level and carotenoid accumulation (Wu et al., 2011; Zhang et al., 2012).

In *Y. lipolytica*, low nitrogen levels can lead to an upregulation of the ergosterol pathway and increased ergosterol accumulation (Kerkhoven et al., 2016, 2017), with the transcription factor Mhy1 indicated as having a role in regulating the steroid biosynthesis pathway (Wang et al., 2018). Other transcription factors that regulate lipid production, such as Mig1 or Mga2, may also have effects on the transcription of MVA pathway genes (Wang et al., 2013; Liu et al., 2015; Morin et al., 2011). Interestingly, the translation elongation factor-1α promoter used to constitutively express the engineered genes was shown to have varying activity during cultivation with high activity under late-stage cultivation and low nitrogen conditions (Liu et al., 2019). Increased transcription of downstream MVA enzymatic steps during late stage fermentations may help alleviate potential pathway bottlenecks. In addition, several MVA pathway enzymes are known to have metabolite feedback inhibition mechanisms, including MVA kinase, which is highly inhibited by GPP and FPP (Miziorko, 2011). Thus, the rate-limiting step may be due to interactions between multi-level cellular responses under stressed fermentation conditions. Decreased levels of GPP and FPP measured over the course of the fermentation may alleviate inhibition of MVA kinase, leading to higher MVA utilization. Overall, the resulting 4-fold increase in rate during the production phase indicates a shift in metabolism to consume MVA and produce ionone more quickly than would be possible through MVA biosynthesis alone without additional engineering efforts.

Both yeast and *E. coli* have been reported to secrete MVA when engineered to overexpress the MVA pathway. However, whereas some intermediates are secreted and then taken up for enhanced productivity, e.g., IPP in *E. coli* (George et al., 2018), the uptake of MVA has not been reported to enable ionone production. Ionone production studies in *E. coli* have indicated more rapid ionone accumulation during the stationary phase, but as extracellular MVA was not measured, the cause of the increase was not determined (Zhang et al., 2018; Chen et al., 2019). Perhaps it is not surprising that *Y. lipolytica* is capable of using exogenous MVA, as its capacity to take up secreted metabolites like pyruvate (Yovkova et al., 2014) and acetate

(Gao et al., 2016a) over the course of fermentation is well known, with another study describing the secretion of the precursor dammarenediol-II during the production of protopanaxadiol that has a subsequent reduction of the extracellular precursor concentration (Wu et al., 2019). Citric acid secretion and uptake after glucose exhaustion has also been observed in fermenters under varying conditions (Sabra et al., 2017). These studies indicate that the flexible metabolism of *Y. lipolytica* may present an advantage for high-cell-density cultivation relative to other species. Although the exact mechanism resulting in uptake remains under study, the temporal metabolic shifts of engineered strains in fermenters are intriguing and may provide guidelines for strain engineering. For example, several other oleaginous yeast and fungi have been reported to display similar lipid turnover dynamics during fermentation as *Y. lipolytica*, such as *Cunninghamella echinulata* and *Cryptococcus podzolicus* (Fakas et al., 2007; Qian et al., 2019) and in *Saitoella coloradoensis* and several *Lipomyces* species (Slininger et al., 2016).

Changes in TCA Cycle Metabolite Levels and Activity Further Suggest Altered Metabolism over the Course of Fed-Batch Fermentations

The decrease in TCA metabolite pool sizes and the limited label incorporation suggest that the TCA cycle has a decreased role during fermentations. It has been previously reported that the TCA cycle can be incomplete during aerobic growth in high-cell-density *E. coli* fermentations (Chen et al., 2011). During cultivations, dissolved oxygen becomes scarce, resulting in reduced electron transport and reduced TCA cycle metabolism. As *Y. lipolytica* is an obligate aerobe, the limited oxygen availability could result in decreased TCA cycle and cellular metabolic activity. Previous studies have shown that low oxygen availability reduces isocitrate, CIT, and AKG formation in *Y. lipolytica* (Sabra et al., 2017; Kamzolova et al., 2012, 2013; Bellou et al., 2014). During growth on glucose, the dissolved oxygen content has an increased effect on the amount of CIT produced relative to growth on other carbon sources (Sabra et al., 2017; Magdouli et al., 2018). Flux balance analysis modeling supported the suppression of the TCA cycle under conditions that still had oxygen uptake (Figure S7), which combined with previous experimental results indicates that TCA cycle functionality is highly sensitive to oxygen levels (Sabra et al., 2017; Magdouli et al., 2018). Three *Y. lipolytica* models iYLI647 (Mishra et al., 2018), iYali4 (Kerkhoven et al., 2016), and iMK735 (Kavščcek et al., 2015) were tested and confirmed the *in silico* reduction of the TCA cycle activity with different oxygen uptake rates leading to the inactivation (Figure S7). It is interesting to note that TCA cycle metabolite decreases were not found for CIT, MAL, and FUM during shake-flask cultivation of the Crabtree-positive, natural carotenoid producer, *Xanthophyllomyces dendrorhous* (Alcalde and Fraser, 2018), but decreases were shown for lycopene-producing *Y. lipolytica* (Zhao et al., 2017), further suggesting a unique response of *Y. lipolytica* to oxygen scarcity.

Although evidence may support the reduced role of the TCA cycle during fermentations, other mechanisms and factors may contribute to the decreases in TCA cycle intermediates during the production phase. Some examples include (1) uptake of previously secreted TCA metabolites, which can reduce the need for *Y. lipolytica* to maintain large pool sizes and lead to diluted labeling; (2) dilution from relatively large pool sizes of TCA metabolites in both mitochondria and cytosol; and (3) increased diversion of carbon to products. In addition, *Yarrowia* may undergo a yeast-to-hyphae transition under low oxygen levels or fermentation stresses, leading to both metabolic alterations and morphological changes (Bellou et al., 2014).

Metabolic stress may also contribute to the low oxidative phosphorylation efficiency (Wu et al., 2016). Stress-induced metabolites such as carotenoids (e.g., beta carotene) can partition to the cell membrane (Wang et al., 2019) and damage cell membrane integrity (Verwaal et al., 2010; Liu et al., 2016). Prior work indicates that strains producing high levels of beta carotene are less stable than those grown for ionone production (Czajka et al., 2018), which could also be tied to differences in ATP demands fulfilled by electron transport. A recent study conducted in *E. coli* determined that an IPP-ATP complex was formed in IPP-overexpressing cells, and that the energy of cells dropped to a value of 0.40 from ~0.80 during the fermentation (George et al., 2018). Although attempts to quantify the IPP-ATP complex were not made in this study, it may also contribute to the observed low energy charge (EC) state.

Limitations of the Study

Isotopic pulse-tracing methods cannot completely quantify and decipher all metabolic fluxes. However, ^{13}C-metabolic flux analysis could not be applied as (1) the engineered strain requires complex, rich medium for growth and (2) unknown flux exchange routes exist among cellular compartments. In addition, although controls were used as described throughout the text, the quenching solution may not completely

halt metabolism, which can add variability to the measurements (Figure S4). More comprehensive analyses (including transcriptomics, proteomics, metabolite overflow kinetics, and cell imaging) could reveal the cellular metabolic regulation during ionone fermentation. During ^{13}C-pulse-tracing experiments, cells were sampled from the reactor and labeled with ^{13}C-glucose under shake-flask conditions. The *ex situ* labeling may have unavoidable influence on cell metabolism.^{13}C-pulse-tracing methods can adequately capture the activities of pathways; however, inactive pools and the high interaction of terpene synthesis with lipid metabolism may further confound the results (Liu et al., 2019).

METHODS

All methods can be found in the accompanying Transparent Methods supplemental file.

SUPPLEMENTAL INFORMATION

Supplemental Information can be found online at https://doi.org/10.1016/j.isci.2020.100854.

ACKNOWLEDGMENTS

Arch Innotek has been funded by NIH (1R41GM13027701) and NSF (IIP1722313) STTR grants. We thank Dr. Edward Baidoo for his valuable insights on performing metabolite identification in yeast systems, Dr. Kimberly Parker for instrument use, and the Proteomics and Mass Spectrometry Core Facility at the Donald Danforth Plant Science Center and the United States Department of Agriculture, Agricultural Research Service, for access and use of instrumentation and resources. In addition, we acknowledge support from the National Science Foundation (NSF-MCB #1616820 and NSF-DBI #1427621), the latter grant provided support for acquisition of the QTRAP LC-MS/MS used in this project, and the United States Department of Agriculture, National Institute of Food and Agriculture (USDA-NIFA #2016-67013-24585, 2017-67013-26156, and 2018-33610-28262).

AUTHOR CONTRIBUTIONS

Conceptualization, D.K.A. and Y.J.T.; Methodology, J.J.C. and S.K.; Investigation, J.J.C. and Y.W.; Formal Analysis, J.J.C. and S.K.; Writing – Original Draft, J.J.C.; Writing – Review & Editing, Y.J.T., D.K.A., S.K., and J.J.C.; Visualization, J.J.C. and S.K.; Supervision, D.K.A., Y.W., and Y.J.T; Funding Acquisition, Y.W.

DECLARATION OF INTERESTS

Y.W. is founder of Arch Innotek and company CSO. Y.W. has the related patent:

Wang Y. 2019. Compositions and methods of biosynthesizing carotenoids and their derivatives. US patent number 10364434.

The authors declare no other competing interests.

Received: September 28, 2019
Revised: December 19, 2019
Accepted: January 15, 2020
Published: February 21, 2020

REFERENCES

Abernathy, M.H., Czajka, J.J., Allen, D.K., Hill, N.C., Cameron, J.C., and Tang, Y.J. (2019). Cyanobacterial carboxysome mutant analysis reveals the influence of enzyme compartmentalization on cellular metabolism and metabolic network rigidity. Metab. Eng. *54*, 222–231.

Alcalde, E., and Fraser, P.D. (2018). Extending our tools and resources in the non-conventional industrial yeast *Xanthophyllomyces dendrorhous* through the application of metabolite profiling methodologies. Metabolomics *14*, 30.

Allen, D.K. (2016). Quantifying plant phenotypes with isotopic labeling & metabolic flux analysis. Curr. Opin. Biotechnol. *37*, 45–52.

Allen, D.K., and Ratcliffe, R.G. (2009). Quantification of isotope label. In Plant Metabolic Networks, J. Schwender, ed. (Springer), pp. 105–150.

Bellou, S., Makri, A., Triantaphyllidou, I.E., Papanikolaou, S., and Aggelis, G. (2014). Morphological and metabolic shifts of *Yarrowia lipolytica* induced by alteration of the dissolved oxygen concentration in the growth environment. Microbiology *160*, 807–817.

Calo, P., de Miguel, T., Velázquez, J.B., and Villa, T.G. (1995). Mevalonic acid increases trans-astaxanthin and carotenoid biosynthesis in Phaffia rhodozyma. Biotechnol. Lett. *17*, 575–578.

Campbell, K., Xia, J., and Nielsen, J. (2017). The impact of systems biology on bioprocessing. Trends Biotechnol. *35*, 1156–1168.

Chen, X., Alonso, A.P., Allen, D.K., Reed, J.L., and Shachar-Hill, Y. (2011). Synergy between

(13)C-metabolic flux analysis and flux balance analysis for understanding metabolic adaptation to anaerobiosis in E. coli. Metab. Eng. *13*, 38–48.

Chen, X., Shukal, S., and Zhang, C. (2019). Integrating enzyme and metabolic engineering tools for enhanced β-ionone production. J. Agric. Food Chem. *67*, 13451–13459.

Czajka, J.J., Nathenson, J.A., Benites, V.T., Baidoo, E.E.K., Cheng, Q., Wang, Y., and Tang, Y.J. (2018). Engineering the oleaginous yeast Yarrowia lipolytica to produce the aroma compound β-ionone. Microb. Cell Fact. *17*, 136.

Elena, S.F., and de Visser, J.A.G.M. (2003). Environmental stress and the effects of mutation. J. Biol. *2*, 12.

Fakas, S., Galiotou-Panayotou, M., Papanikolaou, S., Komaitis, M., and Aggelis, G. (2007). Compositional shifts in lipid fractions during lipid turnover in Cunninghamella echinulata. Enzyme Microb. Technol. *40*, 1321–1327.

Friedlander, J., Tsakraklides, V., Kamineni, A., Greenhagen, E.H., Consiglio, A.L., Macewen, K., Crabtree, D.V., Afshar, J., Nugent, R.L., Hamilton, M.A., et al. (2016). Engineering of a high lipid producing *Yarrowia lipolytica* strain. Biotechnol. Biofuels *9*, 77.

Gao, C., Yang, X., Wang, H., Rivero, C.P., Li, C., Cui, Z., Qi, Q., and Lin, C.S.K. (2016a). Robust succinic acid production from crude glycerol using engineered Yarrowia lipolytica. Biotechnol. Biofuels *9*, 179.

Gao, X., Gao, F., Liu, D., Zhang, H., Nie, X., and Yang, C. (2016b). Engineering the methylerythritol phosphate pathway in cyanobacteria for photosynthetic isoprene production from CO2. Energy Environ. Sci. *9*, 1400–1411.

George, K.W., Thompson, M.G., Kim, J., Baidoo, E.E.K., Wang, G., Benites, V.T., Petzold, C.J., Chan, L.J.G., Yilmaz, S., Turhanen, P., et al. (2018). Integrated analysis of isopentenyl pyrophosphate (IPP) toxicity in isoprenoid-producing Escherichia coli. Metab. Eng. *47*, 60–72.

Halket, J.M., Waterman, D., Przyborowska, A.M., Patel, R.K., Fraser, P.D., and Bramley, P.M. (2005). Chemical derivatization and mass spectral libraries in metabolic profiling by GC/MS and LC/MS/MS. J. Exp. Bot. *56*, 219–243.

Hsiao, J.J., Potter, O.G., Chu, T.W., and Yin, H. (2018). Improved LC/MS methods for the analysis of metal-sensitive analytes using medronic acid as a mobile phase additive. Anal. Chem. *90*, 9457–9464.

Ikeura, R., Murakawa, S., and Endo, A. (1988). Growth inhibition of yeast by compactin (ML-236B) analogues. J. Antibiot. (Tokyo) *41*, 1148–1150.

Jang, C., Chen, L., and Rabinowitz, J.D. (2018). Metabolomics and isotope tracing. Cell *173*, 822–837.

Jiang, R., Chen, X., Lian, J., Huang, L., Cai, J., and Xu, Z. (2019). Efficient production of Pseudoionone with multipathway engineering in Escherichia coli. J. Appl. Microbiol. *126*, 1751–1760.

Kambhampati, S., Li, J., Evans, B.S., and Allen, D.K. (2019). Accurate and efficient amino acid analysis for protein quantification using hydrophilic interaction chromatography coupled tandem mass spectrometry. Plant Methods *15*, 46.

Kamzolova, S.V., Chiglintseva, M.N., Lunina, J.N., and Morgunov, I.G. (2012). alpha-Ketoglutaric acid production by *Yarrowia lipolytica* and its regulation. Appl. Microbiol. Biotechnol. *96*, 783–791.

Kamzolova, S.V., Dedyukhina, E.G., Samoilenko, V.A., Lunina, J.N., Puntus, I.F., Allayarov, R.L., Chiglintseva, M.N., Mironov, A.A., and Morgunov, I.G. (2013). Isocitric acid production from rapeseed oil by *Yarrowia lipolytica* yeast. Appl. Microbiol. Biotechnol. *97*, 9133–9144.

Käß, F., Junne, S., Neubauer, P., Wiechert, W., and Oldiges, M. (2014). Process inhomogeneity leads to rapid side product turnover in cultivation of Corynebacterium glutamicum. Microb. Cell Fact. *13*, 6.

Kavšček, M., Bhutada, G., Madl, T., and Natter, K. (2015). Optimization of lipid production with a genome-scale model of Yarrowia lipolytica. BMC Syst. Biol. *9*, 72.

Kerkhoven, E.J., Kim, Y.M., Wei, S., Nicora, C.D., Fillmore, T.L., Purvine, S.O., Webb-Robertson, B.J., Smith, R.D., Baker, S.E., Metz, T.O., and Nielsen, J. (2017). Leucine biosynthesis is involved in regulating high lipid accumulation in *Yarrowia lipolytica*. MBio *8*, e00857–17.

Kerkhoven, E.J., Pomraning, K.R., Baker, S.E., and Nielsen, J. (2016). Regulation of amino-acid metabolism controls flux to lipid accumulation in Yarrowia lipolytica. NPJ Syst. Biol. Appl. *2*, 16005.

Kildegaard, K.R., Adiego-Pérez, B., Doménech Belda, D., Khangura, J.K., Holkenbrink, C., and Borodina, I. (2017). Engineering of *Yarrowia lipolytica* for production of astaxanthin. Synth. Syst. Biotechnol. *2*, 287–294.

Larroude, M., Celinska, E., Back, A., Thomas, S., Nicaud, J.M., and Ledesma-Amaro, R. (2018). A synthetic biology approach to transform *Yarrowia lipolytica* into a competitive biotechnological producer of beta-carotene. Biotechnol. Bioeng. *115*, 464–472.

Li, Z., Han, J., Sun, S.A., Chen, K., and Tang, D.Q. (2016). Hydrophilic interaction liquid chromatography/mass spectrometry: an attractive and prospective method for the quantitative bioanalysis in drug metabolism. Curr. Drug Metab. *17*, 386–400.

Li, Z., Li, Y., Chen, W., Cao, Q., Guo, Y., Wan, N., Jiang, X., Tang, Y.J., Wang, Q., and Shui, W. (2017). Integrating MS1 and MS2 scans in high-resolution parallel reaction monitoring assays for targeted metabolite quantification and dynamic 13C-labeling metabolism analysis. Anal. Chem. *89*, 877–885.

Liu, H., Marsafari, M., Deng, L., and Xu, P. (2019). Understanding lipogenesis by dynamically profiling transcriptional activity of lipogenic promoters in Yarrowia lipolytica. Appl. Microbiol. Biotechnol. *103*, 3167–3179.

Liu, L., Markham, K., Blazeck, J., Zhou, N., Leon, D., Otoupal, P., and Alper, H.S. (2015). Surveying the lipogenesis landscape in *Yarrowia lipolytica* through understanding the function of a Mga2p regulatory protein mutant. Metab. Eng. *31*, 102–111.

Liu, P., Sun, L., Sun, Y., Shang, F., and Yan, G. (2016). Decreased fluidity of cell membranes causes a metal ion deficiency in recombinant *Saccharomyces cerevisiae* producing carotenoids. J. Ind. Microbiol. Biotechnol. *43*, 525–535.

Lukin, I., Jach, G., Wingartz, I., Welters, P., and Schembecker, G. (2019). Recovery of natural alpha-ionone from fermentation broth. J. Agric. Food Chem. 13412–13419.

Luo, X.T., Cai, B.D., Jiang, H.P., Xiao, H.M., Yuan, B.F., and Feng, Y.Q. (2019). Sensitive analysis of trehalose-6-phosphate and related sugar phosphates in plant tissues by chemical derivatization combined with hydrophilic interaction liquid chromatography-tandem mass spectrometry. J. Chromatogr. A. *1592*, 82–90.

Magdouli, S., Brar, S.K., and Blais, J.F. (2018). Morphology and rheological behaviour of *Yarrowia lipolytica*: impact of dissolved oxygen level on cell growth and lipid composition. Process Biochem. *65*, 1–10.

Miao, L., Chi, S., Tang, Y., Su, Z., Yin, T., Guan, G., and Li, Y. (2011). Astaxanthin biosynthesis is enhanced by high carotenogenic gene expression and decrease of fatty acids and ergosterol in a *Phaffia rhodozyma* mutant strain. FEMS Yeast Res. *11*, 192–201.

Mishra, P., Lee, N.-R., Lakshmanan, M., Kim, M., Kim, B.-G., and Lee, D.-Y. (2018). Genome-scale model-driven strain design for dicarboxylic acid production in Yarrowia lipolytica. BMC Syst. Biol. *12*, 12.

Miziorko, H.M. (2011). Enzymes of the mevalonate pathway of isoprenoid biosynthesis. Arch. Biochem. Biophys. *505*, 131–143.

Morin, N., Cescut, J., Beopoulos, A., Lelandais, G., Le Berre, V., Uribelarrea, J.L., Molina-Jouve, C., and Nicaud, J.M. (2011). Transcriptomic analyses during the transition from biomass production to lipid accumulation in the oleaginous yeast Yarrowia lipolytica. PLoS One *6*, e27966.

Nagai, H., Masuda, A., Toya, Y., Matsuda, F., and Shimizu, H. (2018). Metabolic engineering of mevalonate-producing *Escherichia coli* strains based on thermodynamic analysis. Metab. Eng. *47*, 1–9.

Papanikolaou, S., Muniglia, L., Chevalot, I., Aggelis, G., and Marc, I. (2002). *Yarrowia lipolytica* as a potential producer of citric acid from raw glycerol. J. Appl. Microbiol. *92*, 737–744.

Qian, X., Gorte, O., Chen, L., Zhang, W., Dong, W., Ma, J., Jiang, M., Xin, F., and Ochsenreither, K. (2019). Co-production of single cell oil and gluconic acid using oleaginous *Cryptococcus podzolicus* DSM 27192. Biotechnol. Biofuels *12*, 127.

Rodriguez, S., Denby, C.M., Van Vu, T., Baidoo, E.E., Wang, G., and Keasling, J.D. (2016). ATP citrate lyase mediated cytosolic acetyl-CoA biosynthesis increases mevalonate production

in Saccharomyces cerevisiae. Microb. Cell Fact. *15*, 48.

Sabra, W., Bommareddy, R.R., Maheshwari, G., Papanikolaou, S., and Zeng, A.P. (2017). Substrates and oxygen dependent citric acid production by *Yarrowia lipolytica*: insights through transcriptome and fluxome analyses. Microb. Cell Fact. *16*, 78.

Schwartz, C., Frogue, K., Misa, J., and Wheeldon, I. (2017). Host and pathway engineering for enhanced lycopene biosynthesis in Yarrowia lipolytica. Front. Microbiol. *8*, 2233.

Slininger, P.J., Dien, B.S., Kurtzman, C.P., Moser, B.R., Bakota, E.L., Thompson, S.R., O'Bryan, P.J., Cotta, M.A., Balan, V., Jin, M., et al. (2016). Comparative lipid production by oleaginous yeasts in hydrolyzates of lignocellulosic biomass and process strategy for high titers. Biotechnol. Bioeng. *113*, 1676–1690.

Teleki, A., Sánchez-Kopper, A., and Takors, R. (2015). Alkaline conditions in hydrophilic interaction liquid chromatography for intracellular metabolite quantification using tandem mass spectrometry. Anal. Biochem. *475*, 4–13.

Verwaal, R., Jiang, Y., Wang, J., Daran, J.M., Sandmann, G., van den Berg, J.A., and van Ooyen, A.J. (2010). Heterologous carotenoid production in *Saccharomyces cerevisiae* induces the pleiotropic drug resistance stress response. Yeast *27*, 983–998.

Wang, C., Yoon, S.H., Jang, H.J., Chung, Y.R., Kim, J.Y., Choi, E.S., and Kim, S.W. (2011). Metabolic engineering of *Escherichia coli* for alpha-farnesene production. Metab. Eng. *13*, 648–655.

Wang, C., Zhao, S., Shao, X., Park, J.-B., Jeong, S.-H., Park, H.-J., Kwak, W.-J., Wei, G., and Kim, S.-W. (2019). Challenges and tackles in metabolic engineering for microbial production of carotenoids. Microb. Cell Fact. *18*, 55.

Wang, G., Li, D., Miao, Z., Zhang, S., Liang, W., and Liu, L. (2018). Comparative transcriptome analysis reveals multiple functions for Mhy1p in lipid biosynthesis in the oleaginous yeast Yarrowia lipolytica. Biochim. Biophys. Acta Mol. Cell Biol. Lipids *1863*, 81–90.

Wang, Y.. 2019. Compositions and methods of biosynthesizing carotenoids and their derivatives. US patent application 15560951.

Wang, Z.P., Xu, H.M., Wang, G.Y., Chi, Z., and Chi, Z.M. (2013). Disruption of the MIG1 gene enhances lipid biosynthesis in the oleaginous yeast *Yarrowia lipolytica* ACA-DC 50109. Biochim. Biophys. Acta *1831*, 675–682.

Wehrs, M., Tanjore, D., Eng, T., Lievense, J., Pray, T.R., and Mukhopadhyay, A. (2019). Engineering robust production microbes for large-scale cultivation. Trends Microbiol. *27*, 524–537.

Wu, G., Yan, Q., Jones, J.A., Tang, Y.J., Fong, S.S., and Koffas, M.A.G. (2016). Metabolic burden: cornerstones in synthetic biology and metabolic engineering applications. Trends Biotechnol. *34*, 652–664.

Wu, W., Lu, M., and Yu, L. (2011). Expression of carotenogenic genes and astaxanthin production in *Xanthophyllomyces dendrorhous* as a function of oxygen tension. Z. Naturforsch C J. Biosci. *66*, 283–286.

Wu, Y., Xu, S., Gao, X., Li, M., Li, D., and Lu, W. (2019). Enhanced protopanaxadiol production from xylose by engineered Yarrowia lipolytica. Microb. Cell Fact. *18*, 83.

Xia, Y.G., Yu, L.S., Liang, J., Yang, B.Y., and Kuang, H.X. (2019). Chromatography and mass spectrometry-based approaches for perception of polysaccharides in wild and cultured fruit bodies of Auricularia auricular-judae. Int. J. Biol. Macromol *137*, 1232–1244.

Xu, P., Qiao, K., Ahn, W.S., and Stephanopoulos, G. (2016). Engineering *Yarrowia lipolytica* as a platform for synthesis of drop-in transportation fuels and oleochemicals. Proc. Natl. Acad. Sci. U S A *113*, 10848–10853.

Yoon, S.H., Lee, Y.M., Kim, J.E., Lee, S.H., Lee, J.H., Kim, J.Y., Jung, K.H., Shin, Y.C., Keasling, J.D., and Kim, S.W. (2006). Enhanced lycopene production in *Escherichia coli* engineered to synthesize isopentenyl diphosphate and dimethylallyl diphosphate from mevalonate. Biotechnol. Bioeng. *94*, 1025–1032.

Yovkova, V., Otto, C., Aurich, A., Mauersberger, S., and Barth, G. (2014). Engineering the alpha-ketoglutarate overproduction from raw glycerol by overexpression of the genes encoding NADP+-dependent isocitrate dehydrogenase and pyruvate carboxylase in Yarrowia lipolytica. Appl. Microbiol. Biotechnol. *98*, 2003–2013.

Zhang, C., Chen, X., Lindley, N.D., and Too, H.P. (2018). A "plug-n-play" modular metabolic system for the production of apocarotenoids. Biotechnol. Bioeng. *115*, 174–183.

Zhang, L., Ma, G., Kato, M., Yamawaki, K., Takagi, T., Kiriiwa, Y., Ikoma, Y., Matsumoto, H., Yoshioka, T., and Nesumi, H. (2012). Regulation of carotenoid accumulation and the expression of carotenoid metabolic genes in citrus juice sacs in vitro. J. Exp. Bot. *63*, 871–886.

Zhao, C., Gao, Q., Chen, J., Wei, L., Imanaka, T., and Hua, Q. (2017). Metabolomic changes and metabolic responses to expression of heterologous biosynthetic genes for lycopene production in Yarrowia lipolytica. J. Biotechnol. *251*, 174–185.

iScience, Volume *23*

Supplemental Information

Application of Stable Isotope Tracing to Elucidate Metabolic Dynamics During *Yarrowia lipolytica* α-Ionone Fermentation

Jeffrey J. Czajka, Shrikaar Kambhampati, Yinjie J. Tang, Yechun Wang, and Doug K. Allen

Supplementary Figures and Tables.

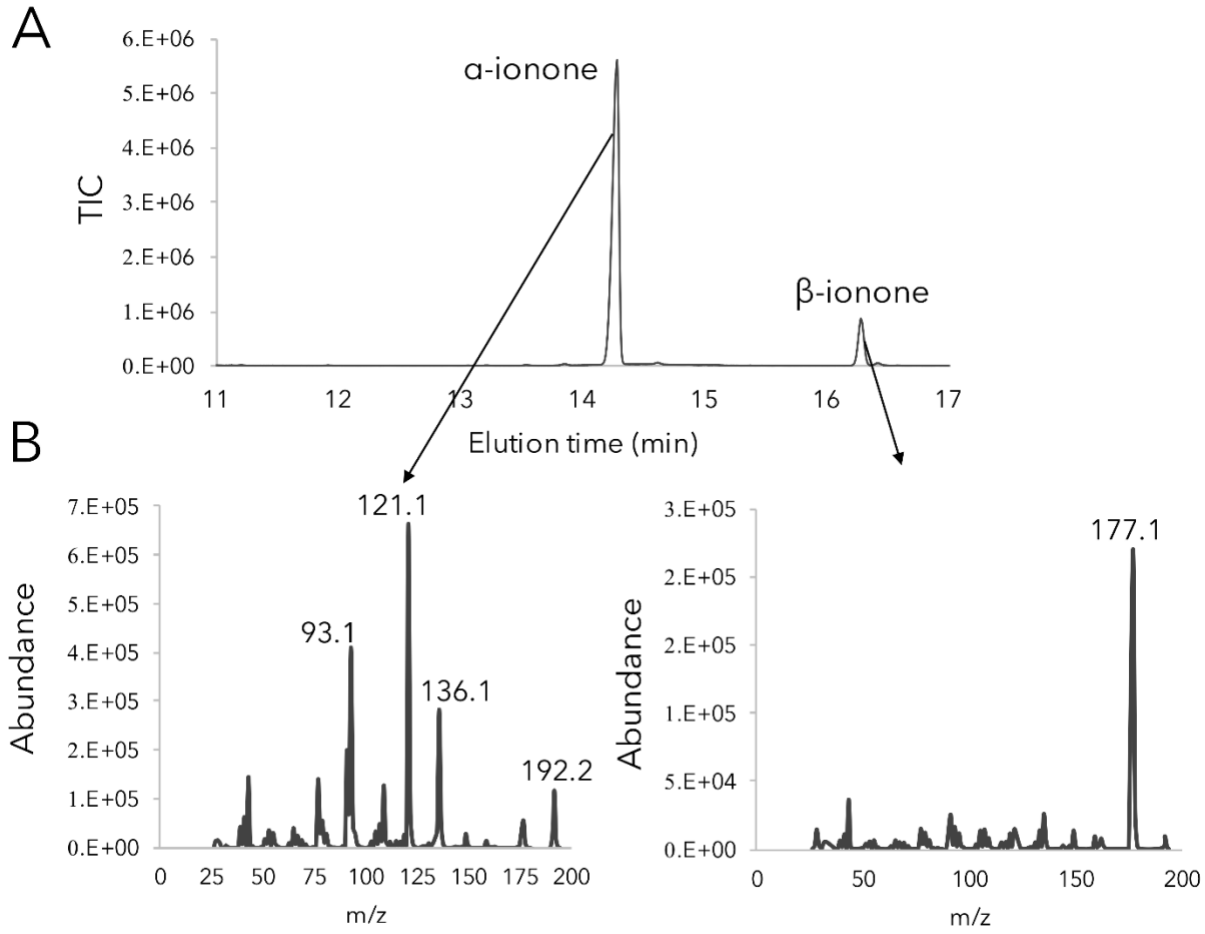

Figure S1, Related to Figure 2. α-ionone detection via GC-MS. (**A)** GC total ion chromatogram analysis from the dodecane overlay of shake-flask α-ionone cultivation. (**B)** α- and β-ionone MS peaks, respectively.

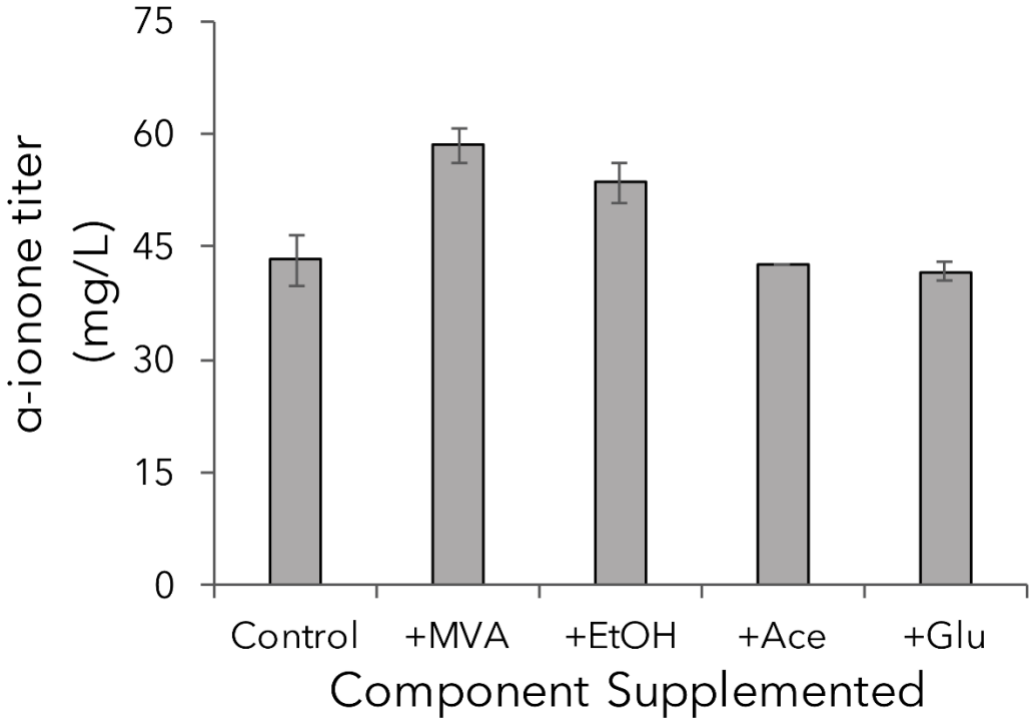

Figure S2, Related to Figure 2. α-ionone titers from shake-flask cultures supplemented with mevalonate (MVA), ethanol (EtOH), acetate (Ace) and glutamate (Glu). Data are represented as mean ± SD from biological triplicates.

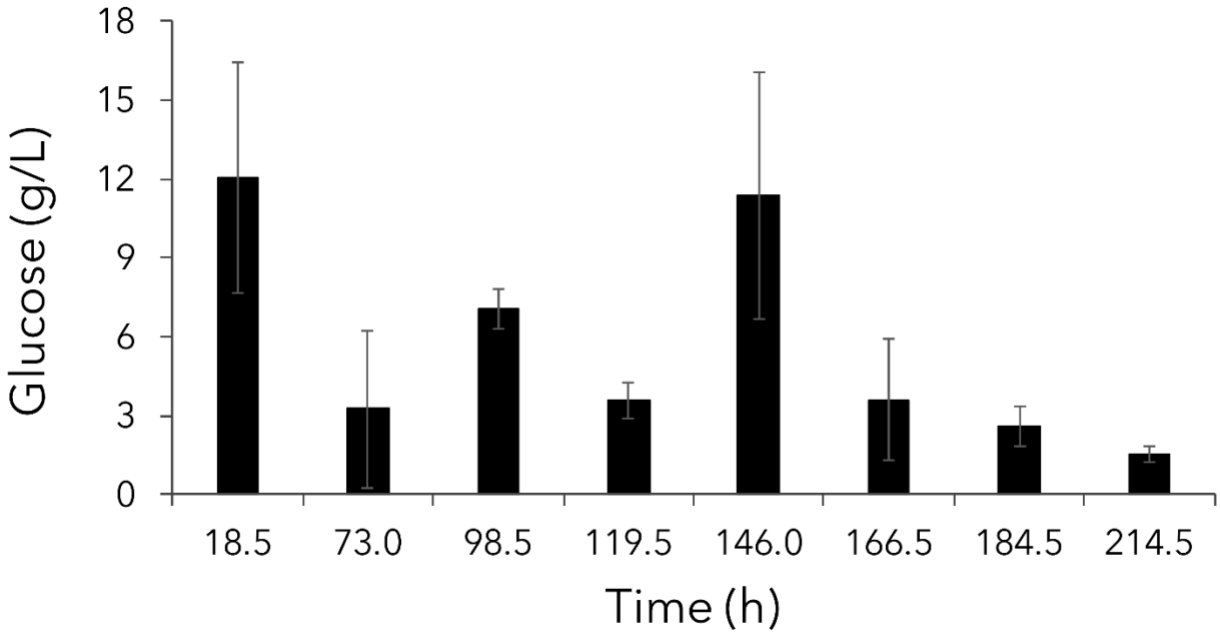

Figure S3, Related to Figure 2. Representative residue glucose in 5 L fermenter. Data are represented as mean ± SD from technical duplicates.

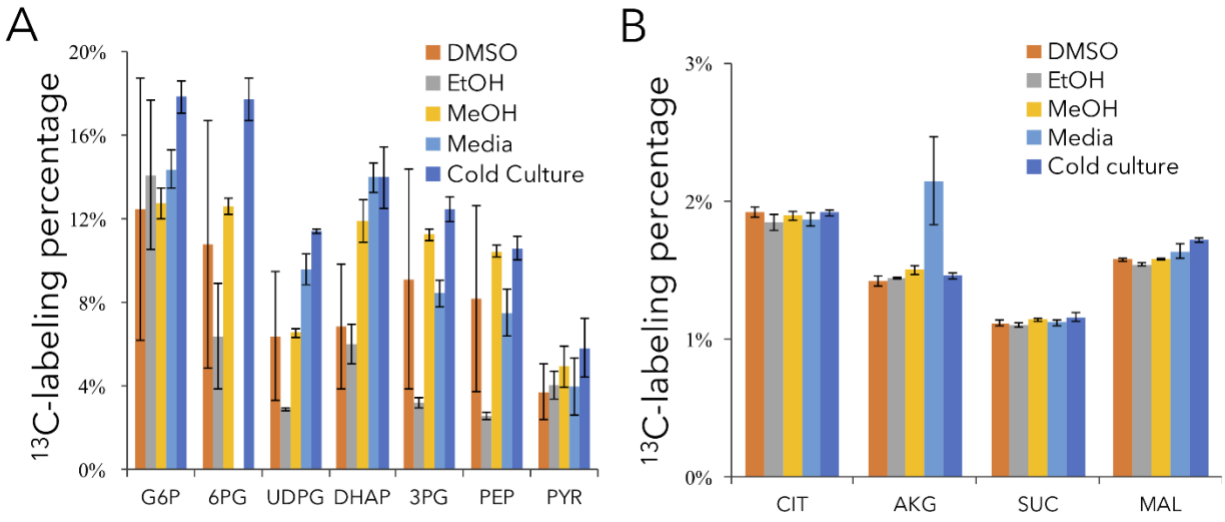

Figure S4, Related to Figure 3, Figure S5 and Figure S6. Quenching verification. DMSO, EtOH, and MeOH refer to the organic component in the quenching solution (60:40 organic:1.35% sodium chloride, final solution temperature ~ -20°C). The "Media" points were quenched using a cold-medium that was rapidly cooled (~0°C) in a liquid N_2 bath. The "Cold Culture" points were cells that were equilibrated at 4°C for 1 hour before pulsing for 30 mins with fully labeled glucose as a comparison of cellular activity at low temperatures. 6PG was not detected in the "Media" quenched samples. **(A)** Glycolytic metabolites and **(B)** TCA cycle metabolites. The EtOH quenching medium was selected for further experiments. Data are represented as mean ± SD from biological triplicates.

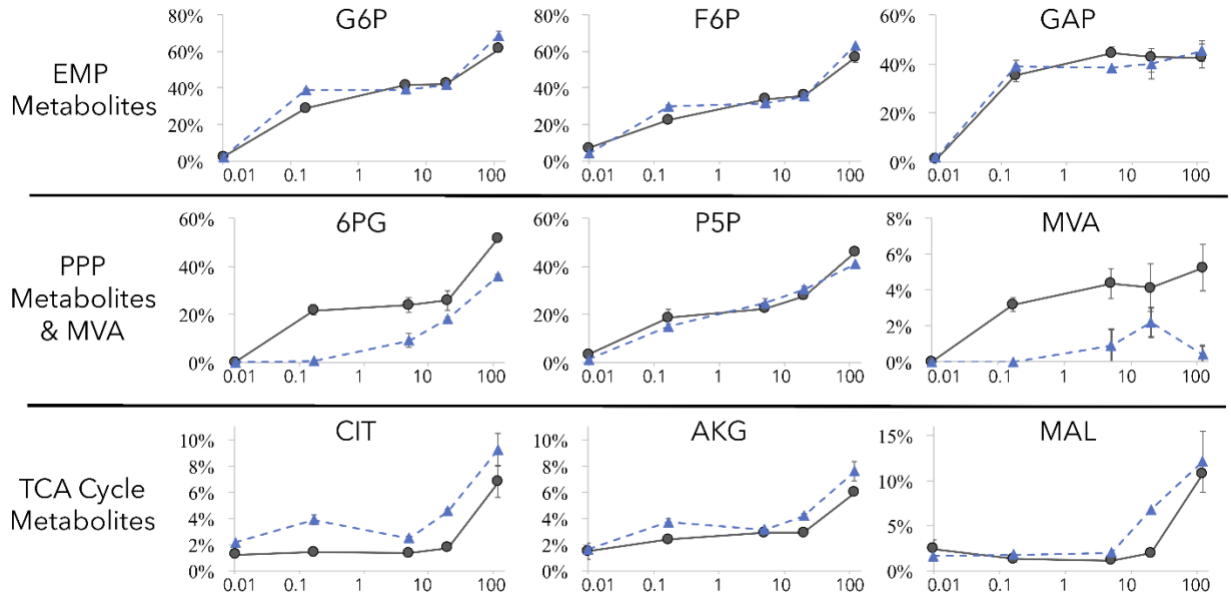

Figure S5. Related to Figure 3. Metabolite labeling in 5 L bioreactor pulse experiments. Y-axis is the labeling percentage of each metabolite, X-axis is the time (min) cells were exposed to the labeled glucose pulse. Growth phase (grey circles, solid line) was sampled at 18.5 h and the production phase (blue triangles, dotted line) was sampled at 119.5 h. Data are represented as mean ± SD from biological duplicates.

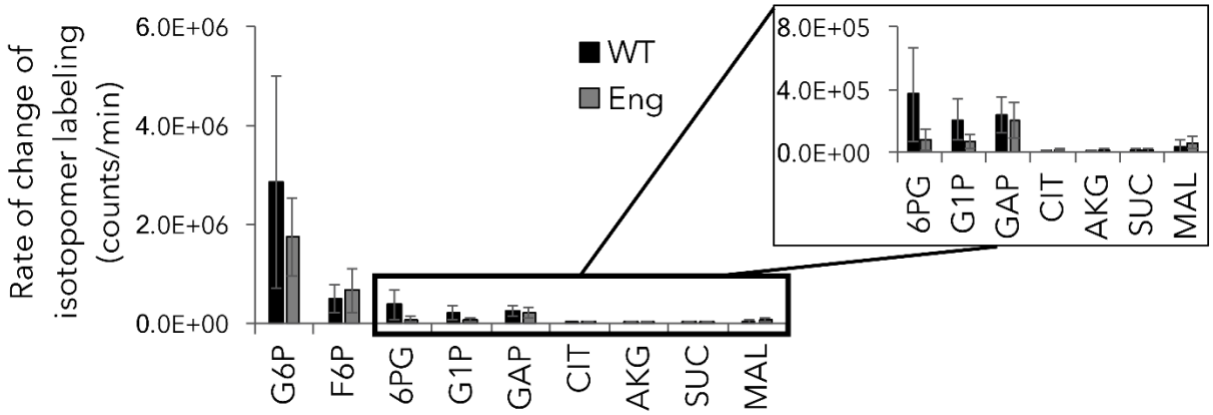

Figure S6, Related to Figure 3 and Figure S5. Max rate of isotopomer labeling change for each metabolite. The rate of labeling change was calculated from the absolute count of the m+6 (for the upper glycolysis metabolites), m+3 (for GAP) and m+2 isotopomers (for TCA cycle metabolites). The rate of change for the upper glycolysis metabolites was the calculated from the early time points (0-30 s), while the TCA cycle labeling rate was the calculated from the 5 to 20 min time-course samples.

Rate of labeling changes are calculated as following:

$R = dm_i/dt = (m_{i,t2} - m_{i,t1}) / \Delta t$

where m_i is the isotopomer and Δt refers to the labeling time. Data are represented as mean ± SD from biological triplicates.

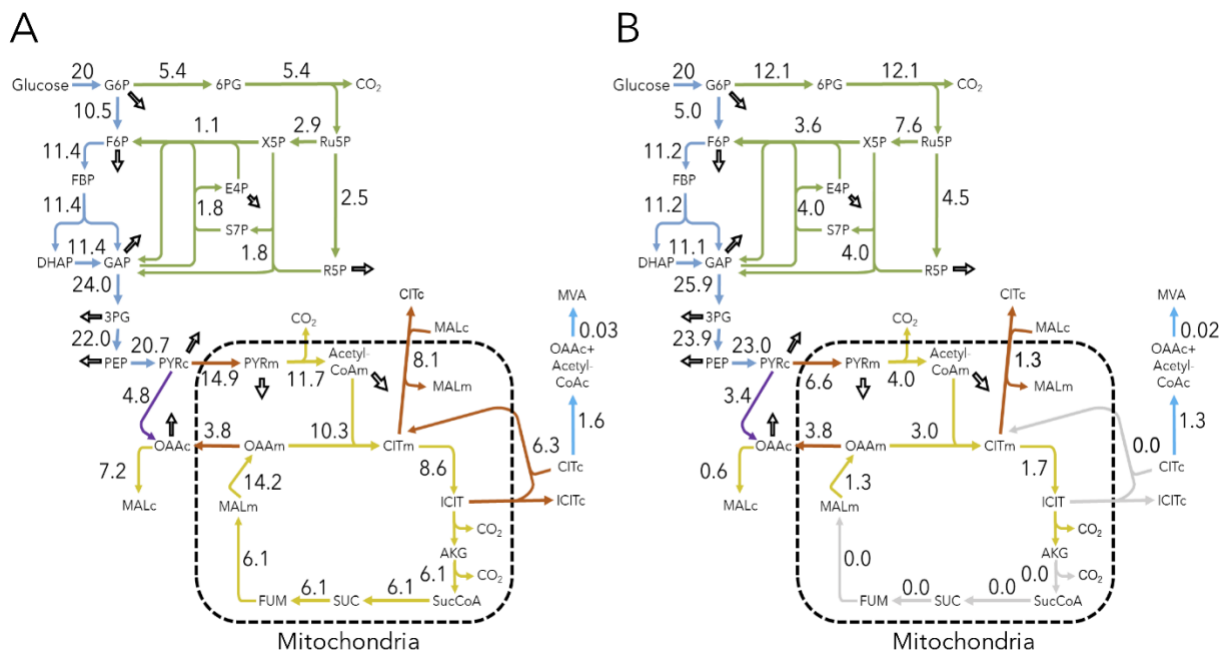

Figure S7, Related to Figure 3 and 5. Intracellular flux simulation from model iMK735 grown under **(A)** O_2 sufficient conditions (O_2 uptake rate = 30 mmol/gDCW/h) and **(B)** low O_2 availability (O_2 uptake rate = 18 mmol/gDCW/h). Flux values are presented in mmol/gDCW/h. Reactions are color coded according to biochemical pathway (blue = glycolysis, green = PP pathway, yellow = TCA cycle, brown = transport reactions, purple = anaplerotic reactions. Grey arrows represent reactions with no flux). “c” or “m” after metabolite names denote cytosolic or mitochondrial pools, respectively.

Table S1. Metabolite parameters for HILIC-based MS detection, Related to Figure 1.

	Metabolite	L.O.D (pmol)	Retention Time (min)	Collision Energy (eV)	Q1 Mass	Q3 Mass	Correlation Coefficient
Sugar Phosphates	2-PG	1.21	9.6	-20	155	79	0.874
	2-PGA	2.99	10.4	-20	185	79	0.870
	3-PGA	0.52	9.1	-20	185	79	0.839
	6-PG	0.78	9.7	-22	275	79	0.882
	ADPG	0.09	7.6	-32	588	346	0.947
	DHAP	3.01	10.6	-14	169	97	0.861
	E4P	0.57	8.3	-32	199	97	0.904
	FBP	1.29	10.7	-24	339	97	0.928
	G1P	2.66	8.7	-28	259	79	0.944
	G6P	2.46	9.0	-20	259	97	0.879
	GAP	4.96	8.2	-14	169	97	0.856
	PEP	2.42	9.9	-14	167	79	0.852
	PIPES	0.26	6.6	-34	301	193	0.943
	P5P	3.82	8.4	-50	229	97	0.837
	RUBP	1.23	10.8	-66	309	97	0.913
	S7P	2.36	8.6	-58	289	97	0.859
	UDPG	0.10	7.5	-32	565	323	0.941
Organic Acids	AKG	7.04	7.7	-12	145	101	0.879
	FUM	0.54	8.5	-10	115	71	0.893
	Glyoxylate	9.36	2.8	-12	73	45	0.881
	Glycerate	0.12	4.5	-16	105	75	0.956
	Glycolate	52.31	4.4	-12	75	47	0.867
	MAL	0.01	8.4	-20	133	115	0.861
	PYR	1.50	2.3	-10	87	43	0.982
	SUC	25.82	8.0	-16	117	73	0.837
Sugars	Fructose	0.85	3.7	-10	179	89	0.981
	Galactinol	0.21	9.2	-18	341	179	0.944
	Glucose	0.05	4.4	-10	179	89	0.985
	Maltose	1.81	7.5	-10	341	161	0.882
	Raffinose	1.33	7.0	-28	503	179	0.951
	Ribitol	0.39	3.2	-16	151	89	0.964

	Sucrose	0.47	5.7	-18	341	179	0.948
MVA Intermediates	MVA	2.41	3.8	-18	147	59	0.980
	MVAP	0.39	8.9	-54	227	49	0.998
	MVAPP	1.33	9.7	-62	306	79	0.961
	IPP	1.25	7.0	-20	245	79	0.970
	GPP	3.17	5.0	-46	313	79	0.972
	FPP	1.84	4.4	-76	381	79	0.939
	GGPP	2.81	4.5	-88	449	79	0.979
Energy Molecules	ADP	0.44	8.7	-31.7	426	134	0.973
	AMP	0.34	7.8	-43.9	346	134	0.996
	ATP	1.84	9.2	-39	506	159	0.933
Amino Acids	Ala	29.86	5.7	43	90	44	0.831
	Asn	2.42	6.4	46	133	74	0.732
	Asp	1.87	7.6	17	134	74	0.932
	(Cys)2	2.24	8.6	19	241.2	152.1	0.807
	Gln	3.79	6.3	46	147	56	0.773
	Glu	7.36	7.7	21	148	84	0.732
	Gly	6.47	6.2	19	76	30	0.886
	Ile	4.87	3.9	23	132	69	0.774
	Leu	3.74	3.7	13	132	86	0.946
	Met	6.43	4.1	11	150	104	0.822
	Phe	1.52	3.5	17	166	120	0.943
	Pro	8.29	4.5	21	116	70	0.910
	Ser	7.45	6.4	15	106	60	0.795
	Thr	6.77	5.8	15	120	74	0.683
	Val	5.94	4.4	15	118	72	0.921

Table S2. List of Arch Innotek strains utilized in this study, Related to Figure 2.

Strain	Genotype	Source
WT (CLIB138)	MatB, leu2-35, lys5-12, ura3-18, xpr2LYS5	CIRM-Levures (Thiverval-grignon, France)
AI-78	ssNphT7, hpIPI, pTEF-HMGS-tXPR2, pTEF-tHMGR-tXPR2, pTEF-MK-tXPR2, pTEF-PMK-tXPR2, pTEF-MPD-tXPR2, pTEF-GPS-tXPR2, pTEF-FPPS-GGPPS-tXPR2, pTEF-carRP-carB-tXPR2	Arch Innotek, described in (Czajka et al., 2018)
AI-77	ssNphT7, hpIPI, pTEF-HMGS-tXPR2, pTEF-tHMGR-tXPR2, pTEF-MK-tXPR2, pTEF-PMK-tXPR2, pTEF-MPD-tXPR2, pTEF-GPS-tXPR2, pTEF-FPPS-GGPPS-tXPR2, pTEF-carRP*-carB-tXPR2, pTEF-LsLCYe*-tXPR2, pTEF-OfCCD1-tXPR2	Arch Innotek, described in this work

*Indicates a mutated gene was utilized, property of Arch Innotek.

Transparent Methods

Chemicals and Cultivation Conditions

U-$^{13}C_6$ glucose was obtained from Cambridge Isotope Laboratories (Tewksbury, MA, USA). Glucose enzymatic kits were purchased from Boehringer Mannheim. All other chemicals and reagents were purchased from Sigma-Aldrich (St. Louis, MO, USA) unless otherwise specified. Strains were maintained on YPD plates containing 10 g yeast extract, 20 g peptone, 20 g glucose and 20 g agar per liter. Minimal medium consisted of Yeast-Nitrogen-Base (US Biological Life Sciences) medium with a complete synthetic drop-out mix (US Biological Life Science), 5 g/L ammonium sulfate and 2 g/L glucose. Liquid cultures were grown in 5 mL of YPD medium in shaking tubes or 25 mL of liquid in 250 mL unbaffled shake-flasks for ionone screening. Medium supplementation experiments were performed in 250 mL shake-flasks with 25 mL of YPD medium with 3 mL dodecane and grown for 120 h. At 24 h, cultures were supplemented with 2.5 mL of the appropriate concentrated carbon source, pH adjusted to a range of 6-7, for a final concentration of 2 g/L.

Fermentations

Seed cultures containing 25 mL of YPD medium in unbaffled 250 mL shake-flasks were inoculated from fresh plates (<3 days old) and grown overnight. Fermenters were inoculated to an OD_{600} of ~0.3-0.8. The DO was set to 20% via cascade control of agitation and an air flow of 1/1 vvm was maintained throughout the cultivation. pH was set at 5.5 and controlled via the addition of citric acid and sodium hydroxide. For short fed-batch fermentation studies (up to ~130 h), a 2 L reactor (Eppendorf BioFlo 120 system) with an initial volume of 0.85 L was used. 250 mL of 10 x YPD medium was initial fed at a flowrate of 0.2 mL/min, followed by 500 mL of 50% glucose. For fermentations >135 h, a 5 L reactor (Sartorius BIOSTAT A system) was employed and had an initial volume of 1.25 L. 500 mL of 10 x YPD medium was initially fed, followed by 1.0 L of 50% glucose at 0.15 mL/min. A 10% (v/v) dodecane layer was maintained through the fermentations.

Metabolite extraction

Metabolite dynamic labeling, pool size measurement and extracellular metabolite data were gathered and confirmed on two different LC-MS systems. All samples were extracted in a 1:1 (v/v) methanol (MeOH):chloroform solution containing acid washed glass beads at 4°C for 6 hours, with the solution vortexed hourly. 0.5 mL of ddH_2O was added and the upper aqueous phase removed and centrifuged in 3KDa filters at 0°C. Samples were then frozen, lyophilized and reconstituted in a 1:1 (v/v) MeOH:ddH_2O solution. 5 µM of PIPES was added as an internal standard prior to the extraction and used to normalize samples. Medium samples had an additional 60:30:10 acetonitrile:MeOH:ddH_2O solution added in a 1:1 v/v ratio to the reconstituted sample to precipitate salts and proteins before analysis.

Chromatography and mass spectrometry conditions

A Shimadzu Prominence-xR UFLC system was used for chromatographic separation and a SCIEX hybrid triple quadrupole-linear ion trap MS equipped with Turbo V™ electrospray ionization (ESI) source was used for detection of metabolites. The mobile phase solvents, A and B contained 10 mM ammonium acetate and 5 µM medronic acid in water and 9:1 acetonitrile:ddH_2O, respectively. A 3 µL sample was injected on to an InfinityLab Poroshell 120 HILIC-Z (2.1 x 100 mm, 2.7 µm, Agilent Technologies) column that was held at 40°C, and the following gradient was used: the initial concentration of 95% B was linearly decreased to 70% B over 8 min, and to 50% B over the next 4 min. The gradient was then brought to 30% B over 0.5 min and was held for an additional 1.0 min for clean up before returning to 95% B over 0.5 min. A 6 min equilibration was used to return the column to the starting conditions prior to the next injection. The total runtime was 20 min, and a flowrate of 250 µL/min was used throughout. A polarity switching method was used with sugar phosphates, sugars, organic acids and mevalonate pathway intermediates detected in negative ionization mode and the amino acids in positive ionization mode using a targeted MRM approach. The source conditions used were as follows; ion spray voltage, 4.5 kV (ESI+ and ESI-); ion source temperature, 400°C; source gas 1, 45; source gas 2, 40; and curtain gas, 35. The diagnostic fragments and collision energies used for detection were identified by direct infusion of standards and are presented in Table S1. Data for absolute quantifications were analyzed using the quantitation wizard available in Analyst (v. 1.6.2) software (SCIEX, Concord, Canada). ^{13}C enrichment measurements were quantified via manual integration of peaks.

Quenching verification

Dimethyl sulfoxide, ethanol and MeOH quenching solutions were prepared by mixing in a 60:40 ratio with 1.35% sodium chloride solution as previously described and frozen at -80°C (Zhao et al., 2014). Cultures were grown in 1 L unbaffled shake-flasks with YPD medium. One volume of cell medium was quenched in four times the volume of quenching solution (i.e., 7 mL culture in 28 mL quenching solution, final solution temperature ~ -20°C), pulsed with 1 g/L U-$^{13}C_6$ glucose, and processed for LC-MS/MS analysis as described above. A cold-medium method (Abernathy et al., 2017) was used as a control in which cells were quenched using YNB medium with no carbon source that was rapidly cooled (~0°C) in a liquid N_2 bath. 7 mL cells were also transferred to shaking tubes and equilibrated at 4°C for 1 hour before pulsing for 30 mins with fully labeled glucose and processed for comparison. The ethanol solution was used for all other quenching procedures.

Ionone quantification

Ionone was quantified as previously described (Czajka et al., 2018). Briefly, the dodecane overlay was diluted into hexane and analyzed via GC-MS. Intracellular ionone content was determined by pelleting 0.1 mL of cells, washing with 0.9% sodium chloride and extracting via vortexing in hexane with acid washed glass beads. The concentration was quantified by a standard curve. The GC-MS equipment was an Agilent

Technologies gas chromatography (7820A GC system equipped with a HP-5m column) with a single quadruple mass analyzer (5977E MSD). Ionone retention times were confirmed using both standards and published mass spectrums (Walwil, 2017).

Statistics

WT and engineered pool sizes were collected from biological triplicates. Fermentation parameters were calculated from three separate fermentations. Pool size data over the course of the fermentation was determined from biological duplicates in reactors. Bioreactor culture labeling was conducted on biological duplicates sampled from one fermentation. MVA supplementation data was obtained from biological triplicates. A one-tailed student's T-test was used to test for significance in differences between sample types.

FBA modeling

Modeling was performed in Python using published genome scale models and the COBRApy toolbox (Ebrahim et al., 2013). The GitHub published platform ATOM was utilized (https://atom.io/). The biomass objective function along with reactions that were set to have zero flux are listed below.

Model iYali4. Objective function = 'Biomass production', y000560, 'hydroxymethylglutaryl CoA synthase' (peroxisomal), y002115, 'alcohol dehydrogenase, (acetaldehyde to ethanol)'; y000165, 'mitochondrial alcohol dehydrogenase'; y000719, 'malic enzyme (NADP)'; y002131, 'isocitrate dehydrogenase' (NADP-dependent); y000217, 'aspartate transaminase'.

Model iYLI647. Objective function = 'biomass yarrowia carbon limiting', MGCH, 'Methylglutaconyl-coa hydratase'; FBA3, 'Sedoheptulose 1 7 bisphosphate D glyceraldehyde 3 phosphate lyase'.

Model iMK735. Objective function = 'R_biomass_yarrowia_5.1%_bal_YL'.

Supplemental References

ABERNATHY, M. H., YU, J., MA, F., LIBERTON, M., UNGERER, J., HOLLINSHEAD, W. D., GOPALAKRISHNAN, S., HE, L., MARANAS, C. D., PAKRASI, H. B., ALLEN, D. K. & TANG, Y. J. 2017. Deciphering cyanobacterial phenotypes for fast photoautotrophic growth via isotopically nonstationary metabolic flux analysis. *Biotechnol Biofuels,* 10**,** 273.

EBRAHIM, A., LERMAN, J. A., PALSSON, B. O. & HYDUKE, D. R. 2013. COBRApy: COnstraints-Based Reconstruction and Analysis for Python. *BMC Systems Biology,* 7**,** 74.

WALWIL, A. M. 2017. The Mass Spectra Analysis for α-Ionone and β-Ionone. *International Journal of Chemistry,* 9**,** 61.